Design Modification and Analysis of Brushless Direct-Current Axial Fan Motor Stator Using Taguchi and One-Factor-At-A-Time Method

Ming-Hung Lin[1], Cheng-Che Yang[2], Bo-Wun Huang[2], Jyun-Yi Lin[3], Cheng-Yi Chen[1,*]

[1]Department of Electrical Engineering, Cheng Shiu University, Kaohsiung, Taiwan, ROC

[2]Institute of Mechatronic Engineering, Cheng Shiu University, Kaohsiung, Taiwan, ROC

[3]Department of Mechanical Engineering, National Kaohsiung University of Science and Technology, Kaohsiung, Taiwan, ROC

Received 19 April 2024; received in revised form 23 June 2024; accepted 24 June 2024

DOI: https://doi.org/10.46604/ijeti.2024.13595

Abstract

This paper introduces a novel approach utilizing Altair Flux software for electromagnetic finite element simulation and analyses of cogging torque and back electromotive force (BEMF) without altering the rotor conditions. This investigation aims to understand the effects on the design of brushless direct current (BLDC) axial fan motors. The Altair HyperStudy optimal software is used to conduct the Taguchi experimental method to analyze the influence of critical factors in motor stator design. Subsequently, the one-factor-at-a-time method proposed in this paper is applied to find the optimal motor geometry stator design satisfying the requirements. Eventually, an experimental motor is established and compared with a commercial 9SG5748P5G01 BLDC axial fan motor. The BEMF is resultantly smaller than the 9SG5748P5G01 motor. Furthermore, the disparity between the experimental and simulation analysis results is minimal with consistent findings. The motor stator design and simulation analysis methods can potentially support the motor design.

Keywords: cogging torque, back electromotive force, brushless direct-current motor, axial fan motor

1. Introduction

Given that the applications for motors can range from heavy industries to small toys, the pervasive existence of motors can be undeniably validated. The motors render dichotomous features, i.e., brushed and brushless, which differ in the use of brushes and commutators. Brushless motors, in particular, are perceived to be favorable apropos low noise and easy maintenance, compared to the brushed motors [1-2]. Consequently, brushless motors are emphatically deployed in modern motor applications. However, several challenges, including cogging torque optimization and reduction of magnetic flux density at operational temperatures, emerge from the optimization of motor design. Therefore, future advancements in motor technology purposively focus on operational efficiency, i.e., high speed with better accuracy, and meanwhile smaller size with durability and cost-effectiveness.

In addition, the computing power of electronic devices is directly proportional to the amount of heat generated by the systems in the same space. As a result, the design of fans to increase the level of heat dissipation is especially instrumental. However, this high-density fan design can heighten heat dissipation, incurring a higher resistance in the system, thereby burdening the load of the fans. On the other hand, if expediting the speed of the fan, better heat dissipation with higher pressure

* Corresponding author. E-mail address: k0464@gcloud.csu.edu.tw

English language proofreader: Chih-Wei Chang

and flow rate can be effectuated, whereas both higher power consumption and noise level will ensue as negative consequences. Noise, mainly caused by vibration, can affect the life expectancy of the fan and increase power consumption. Therefore, effectively reducing heat and vibration is considered a critical aspect in the design of fan motors.

Researchers have studied multifarious technological advancements in the electric motor industry. Among relevant studies, the design of electric vehicles has been emphatically investigated [3-5], while the design of electric bicycles and scooters has been attentively examined as well [6-9]. Furthermore, Aishwarya and Brisilla [10] discussed the design of an exceptionally efficient induction motor for electric vehicles, and the design and thermal analysis of an induction motor is conducted in a hydraulic pumping system [11]. Generally, the researchers use finite element analysis software to assist in motor design. Brisset and Brochet [12] used the parameter-constrained sequential quadratic method to optimize the design of the brushless direct current (BLDC) wheel motor. All of them are exploring the areas to reduce the cogging torque of motors, thereby achieving the expected output speed and torque with cost-effectiveness, according to the requirements of the corresponding applications.

Currently, the motor industry is in a mature stage of development. The main issue is to satisfy the tasks using the optimal design under the target situation, and therefore yielding competitiveness in the market. Many researchers have explored methods for the BLDC motor design due to its controllability and widespread applications in industry and daily life. For instance, Das et al. [13] completed the design and fabrication process of the BLDC motor. Despite not operating optimally, this design renders the rationale of BLDC motor design for future works. Singh [14] analyzed the performance of a BLDC motor designed with parameter changes and used ANSYS Maxwell software (AMS) and rotating machine expert (RMxprt) models to reduce cogging torque.

Ren et al. [15] adopted the ANSYS software to design a BLDC motor for automotive cooling fans to improve operating efficiency. Besides, Niaz Azari et al. [16] proposed an optimal BLDC motor design using the Cuckoo optimization algorithm to mitigate losses, construction cost, and motor volume simultaneously. Tosun and Serteller [17] explored the design of the outer-rotor BLDC motor on the investigation of the motor axial-length-to-pole-pitch ratio using AMS. The genetic algorithm process was utilized to identify the significant factors that affect the highest torque, volume, and cogging torque value, optimizing design parameters such as tooth face angle, tooth face radius, and pole arc-to-pole pitch ratio (commutation angle). Sadrossadat and Rahmani [18] introduced a statistical design framework for BLDC motors, considering efficiency maximization with non-linear constraints of flux density, current density, and physical dimensions. The proposed method was attested to perform faster computing results than the Monte Carlo method due to fewer simulations.

Bhuvaneswari et al. [19] optimized the design of an axial flux brushless DC motor for ceiling fan application using a finite element analysis approach, consuming less power for the same airflow. Thakur et al. [20] rendered a design and manufacturing approach for BLDC axial fan to optimize the overall efficiency of mass-flow rate, carried out in ANSYS FLUENT software with a commercial computational fluid dynamics code. The vortex of the fan is shown, and swirls have been reduced compared to the original reference fan. Furthermore, the Taguchi experimental method was utilized to design a single-phase induction fan motor to optimize energy efficiency [21]. This approach provided a substantially small number of experiments for obtaining a compelling design on the design objective.

Based on the erstwhile studies, this paper focuses primarily on the fan model 9SG5748P5G01 from the SanAce172 series as the subject of research available in the market, aiming to develop a brushless DC motor of the same size but with a different stator structure [22]. The optimization of the motor is achieved using FluxMotor and HyperStudy simulation software combined with the Taguchi method. Besides, to address scenarios of reduced starting torque and back electromotive force (BEMF), a one-factor-at-a-time approach is employed to identify the optimal solution, designing better parameters to enhance motor efficiency. Finally, the optimized design results are compared with the 9SG5748P5G01 motor. The basic specifications

of the 9SG5748P5G01 fan motor include a circular casing with flat surfaces at both ends, an outer diameter of approximately 72 mm, and the wind direction downward. Notably, the maximum performance of the fan is 48V input voltage, 2.91A input current, and a maximum speed of 8,600 rpm.

This study applies finite element analysis to investigate cogging torque, BEMF, and torque characteristics of the external rotor brushless DC motor under operational conditions. This paper aims to introduce an improved stator design by defining the geometrical dimensions of the motor's silicon steel components, which reduces cogging effects and achieves the required performance for BEMF and torque. Subsequently, control technology for brushless DC motors will be applied to evaluate the control performance of the designed high-speed (> 8,500 rpm) fan motor. According to the motor improvements, the completion of the FluxMotor simulation results of cogging torque, BEMF, and torque will be used to determine the optimal geometry. Finally, the motor samples are produced and tested to verify the feasibility of the simulation.

2. Optimal Design and Simulation Analysis of the Proposed Motor

The performance of BLDC motors is indeed influenced by design parameters such as slot height, slot width, slot opening width, slot top radius, and slot bottom circle radius [23-25]. According to the motor design theory textbook [26], it's noteworthy that different size factors will affect the transmission of magnetic flux and thus affect the BEMF and torque. Therefore, these parameters are crucial in determining the cogging torque, reluctance torque, BEMF, power, torque, speed, and motor efficiency. In this study, the initial model of the motor without changing the rotor design was established through Altair FluxMotor software. The relevant dimensional parameters were converted into a Python file and imported into Altair Flux for comprehensive configuration. The mesh partitioning process initiates after examining and adjusting the coordinate system of the motor and geometric model parameters. FluxMotor is used to build and parameterize the geometric model according to motor specifications in Table 1.

Table 1 Motor specifications

Parameter	Quantity	Unit
Pole pairs	4	pole
Slot count	6	slot
Rated power	140	W
Rated speed	8600	rpm
Stack thickness	14	mm
Stator outer diameter	59.5	mm
Stator inner diameter	19.8	mm
Rotor outer diameter	72.5	mm
Rotor inner diameter	61	mm
Turns	228	turns

In the modeling process, the design dimensions of various parts of the motor are assigned codes, as shown in Fig. 1, while the geometric dimensions of the reference motor are listed in Table 2. The analysis and design flow chart in this paper is illustrated in Fig. 2.

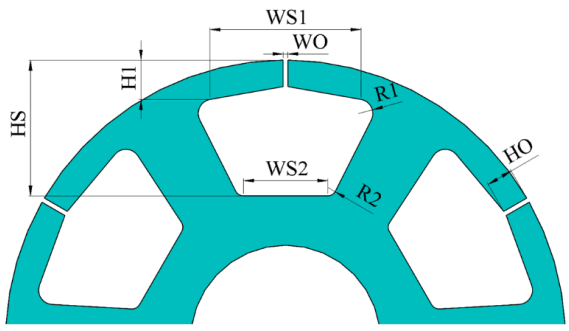

Fig. 1 Motor geometric parameters

Table 2 Motor geometric dimensions

Description and code name	Dimension (mm)
Slot height (HS)	15.3
Intermediary height of the slot (H1)	4.5
Height of slot opening (HO)	1.8
Intermediary width of the slot (WS1)	19.9
Slot width(WS2)	10
Width of slot opening (WO)	2.0
Top slot radius (R1)	1.5
Slot bottom fillet radius (R2)	0.9

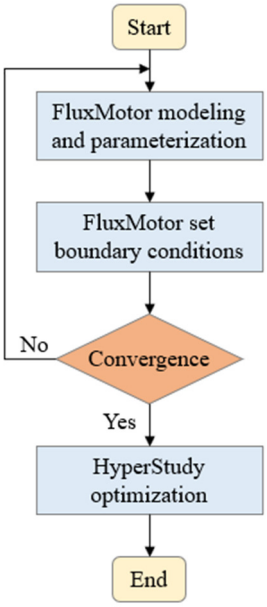

Fig. 2 Analysis and design flow chart

The results are subsequently entered into Flux to set boundary conditions. If the values are reasonable and convergent, HyperStudy will be applied for optimization. In contrast, if convergence is not achieved, the model is returned to FluxMotor for redesign. Rudimentarily, flux is the low-frequency magnetic field analysis module in the Altair suite and is mainly used in finite-element analysis for electromagnetism. The electromagnetic simulations in the Altair software suite are calculated using Flux as a background solver. FluxMotor is a magnetic field analysis software based on Flux that features a friendly interface and simple setup steps using control buttons. The setting steps are simple in building the model and parameterization. The initial simulation results diagrammatically shown are to check if the motor design trend has coincided. HyperStudy is an optimized analysis software developed by Altair. After parameterization, it can be used for experimental analysis and optimal design of the Taguchi method. After acquiring the three most significant parameters, this research utilizes one-factor-at-a-time analysis to obtain the most suitable parameters for motor design.

2.1. Analysis and design of the Taguchi method

The Taguchi method is applied to determine the influence of eight crucial geometric parameters on cogging torque and BEMF in motor stator design. Table 3 describes the control factors of experimental design by using the Taguchi method. These factors are adjusted in a plus or minus 4% deviation range for minor improvement in the original motor performance.

Table 3 Taguchi parameters of each dimension

Description	Level 1	Level 2	Level 3
Factor A (H1)	4.32 mm	4.5 mm	4.68 mm
Factor B (HO)	1.728 mm	1.8 mm	1.872 mm
Factor C (HS)	14.688 mm	15.3 mm	15.912 mm
Factor D (R1)	1.44 mm	1.5 mm	1.56 mm
Factor E (R2)	0.864 mm	0.9 mm	0.936 mm
Factor F (WO)	1.92 mm	2 mm	2.08 mm
Factor G (WS1)	19.104 mm	19.9 mm	20.696 mm
Factor H (WS2)	9.6 mm	10 mm	10.4 mm

Due to a total of 8 factors in the table and each factor having 3 level comparisons, an L27 orthogonal array is deployed to conduct the Taguchi experimental analysis. 27 data sets are calculated from the L27 Taguchi experimental design, as shown in Table 4. Through the solution of cogging torque and BEMF obtained from 27 experiments, eight influence factors analyzed are depicted as follows.

Table 4 Cogging torque and BEMF L27 configuration and data

	H1	HO	HS	R1	R2	WO	WS1	WS2	Cogging torque	BEMF RMS (root mean square)
1	4.32	1.728	14.688	1.44	0.864	1.92	19.104	9.6	0.050	5.658
2	4.32	1.728	14.688	1.44	0.9	2	19.9	10	0.036	5.478
3	4.32	1.728	14.688	1.44	0.936	2.08	20.696	10.4	0.053	5.257
4	4.32	1.8	15.3	1.5	0.864	1.92	19.104	10	0.037	5.397
5	4.32	1.8	15.3	1.5	0.9	2	19.9	10.4	0.062	5.188
6	4.32	1.8	15.3	1.5	0.936	2.08	20.696	9.6	0.054	5.240
7	4.32	1.872	15.912	1.56	0.864	1.92	19.104	10.4	0.086	5.012
8	4.32	1.872	15.912	1.56	0.9	2	19.9	9.6	0.061	5.182
9	4.32	1.872	15.912	1.56	0.936	2.08	20.696	10	0.101	4.938
10	4.5	1.728	15.3	1.56	0.864	2	20.696	9.6	0.058	5.218
11	4.5	1.728	15.3	1.56	0.9	2.08	19.104	10	0.039	5.393
12	4.5	1.728	15.3	1.56	0.936	1.92	19.9	10.4	0.064	5.173
13	4.5	1.8	15.912	1.44	0.864	2	20.696	10	0.106	4.912
14	4.5	1.8	15.912	1.44	0.9	2.08	19.104	10.4	0.088	5.014
15	4.5	1.8	15.912	1.44	0.936	1.92	19.9	9.6	0.063	5.164
16	4.5	1.872	14.688	1.5	0.864	2	20.696	10.4	0.063	5.180
17	4.5	1.872	14.688	1.5	0.9	2.08	19.104	9.6	0.055	5.617
18	4.5	1.872	14.688	1.5	0.936	1.92	19.9	10	0.035	5.416
19	4.68	1.728	15.912	1.5	0.864	2.08	19.9	9.6	0.066	5.154
20	4.68	1.728	15.912	1.5	0.9	1.92	20.696	10	0.111	4.889
21	4.68	1.728	15.912	1.5	0.936	2	19.104	10.4	0.089	5.004
22	4.68	1.8	14.688	1.56	0.864	2.08	19.9	10	0.038	5.405
23	4.68	1.8	14.688	1.56	0.9	1.92	20.696	10.4	0.067	5.153
24	4.68	1.8	14.688	1.56	0.936	2	19.104	9.6	0.049	5.604
25	4.68	1.872	15.3	1.44	0.864	2.08	19.9	10.4	0.071	5.117
26	4.68	1.872	15.3	1.44	0.9	1.92	20.696	9.6	0.071	5.121
27	4.68	1.872	15.3	1.44	0.936	2	19.104	10	0.042	5.345

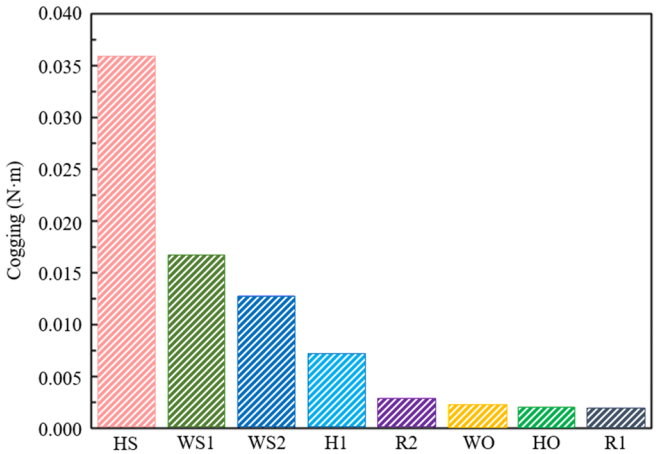

Fig. 3 Influence of various factors on the cogging torque

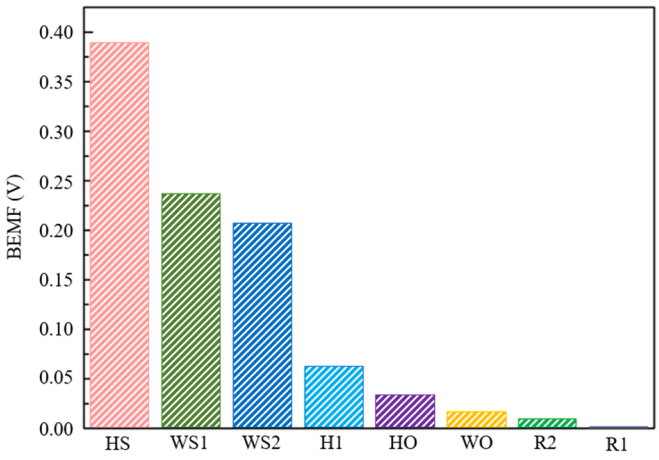

Fig. 4 Influence of various factors on the BEMF

To summarize the aforementioned analysis, Fig. 3 and Fig. 4 are the bar charts of the influence of each factor on cogging torque and BEMF, respectively. From left to right, the chart indicates the influence and is organized in descending order, and the length of the bar is directly proportional to the impact. In addition, the effects of the factors on the cogging torque and the BEMF can be summarized as follows:

(1) increasing the size by H1 results in higher cogging torque and lower BEMF

(2) increasing the size by HO results in higher cogging torque and lower BEMF

(3) increasing the size by HS results in higher cogging torque and lower BEMF

(4) increasing the size by R1 results in lower cogging torque and higher BEMF
(5) increasing size by R2 results in lower cogging torque and higher BEMF
(6) increasing size by HS results in lower cogging torque and higher BEMF
(7) increasing size by WS1 results in higher cogging torque and lower BEMF
(8) increasing size by WS2 results in higher cogging torque and lower BEMF

The effect of each parameter can be organized as the increase in size, i.e., WS1, WS2, H1, HO, and WO results in higher cogging torque and lower BEMF. On the other hand, increasing the size of HS, R2, and R1 results in higher cogging torque and lower BEMF. Given the observations stated above, none of the parameters can lower the cogging torque and the BEMF simultaneously. Therefore, a one-factor-at-a-time approach is used to find out the optimal parameter.

2.2. One-factor-at-a-time design and analysis

Since WS1 and WS2 are slot widths, changing dimensions will significantly affect the slot-filling rate. In this research, the winding number and wire diameter are not modified. The dimensions are not altered due to the changes of R1 and R2 yielding little influence on the cogging torque and BEMF. By removing the above four parameters, a one-factor-at-a-time experiment will be carried out individually for HS, WO, and HO to determine the optimal geometric parameters. The investigation can be divided into three directions; the first is to investigate the effect of different WO dimensions, which render no impact on slot filling rate on cogging torque and BEMF. The second part discusses the effect of different HO dimensions, which yield less impact on slot filling rate on cogging torque and BEMF. The third part is to investigate the effects of different HS dimensions, which can be influenced by HO on cogging torque and BEMF.

2.2.1. Influence of different WO dimensions on torque and BEMF

This section analyzes the cogging torque and BEMF results for different WO sizes of 1.5, 2.0, and 2.5 mm, respectively, as shown in Table 5. To increase the wind speed, reducing BEMF is material to increase the rotating speed. In Table 5, the WO size 1.5 mm BEMF is observed to stand at a lower value, which is more suitable for the demand. However, the cogging torque is increased, compared with the original data.

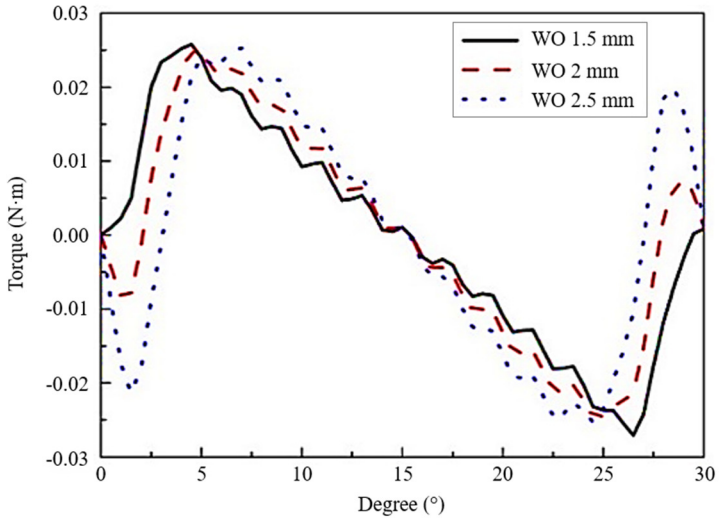

Fig. 5 Cogging torque waveforms of different WO dimensions

Table 5 Cogging torque and BEMF data for different WO dimensions

WO (mm)	Cogging torque (N·m)	BEMF (V)	
1.5	0.0527	Phase1	5.241
		Phase2	5.326
		Phase3	5.317
2.0	0.0516	Phase1	5.271
		Phase2	5.356
		Phase3	5.346
2.5	0.0505	Phase1	5.290
		Phase2	5.374
		Phase3	5.364

From Fig. 5, the waveform of each size is not the same. Although with a higher peak, the waveform of the WO size of 1.5 mm is more harmonic than the waveform of 2.5 mm. Fig. 6 indicates that the waveforms of each size are not significantly different in the BEMF. 1.5 mm is chosen as the fixed factor due to the subsequent parameter adjustment that will be made for the cogging torque.

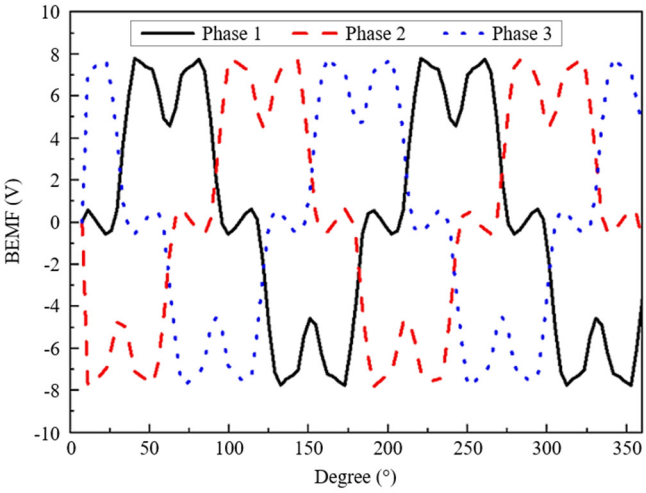

(a) 1.5 mm

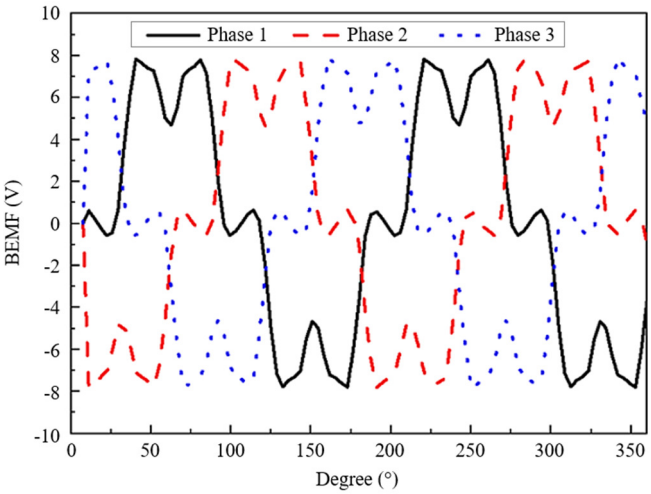

(b) 2 mm

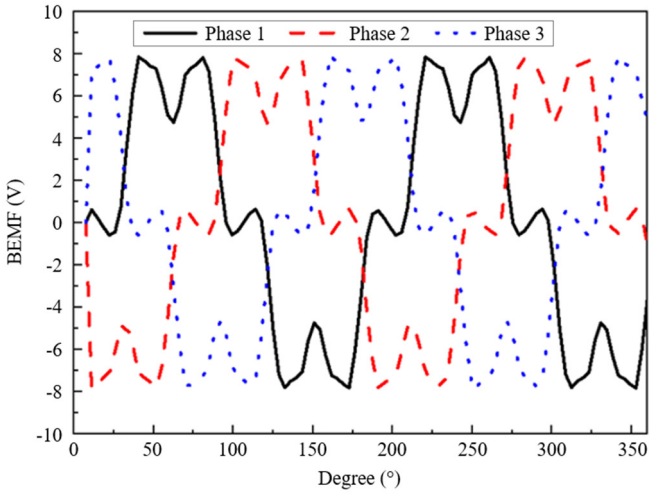

(c) 2.5 mm

Fig. 6 BEMF waveforms for different WO dimensions

2.2.2. *Influence of different HO dimensions on torque and BEMF*

This section primarily examines and analyzes the effects of different HO dimensions on cogging torque and BEMF, especially the sizes of 1.8 mm, 2.0 mm, and 2.4 mm. The data of cogging torque and BEMF at different HO dimensions are presented in Table 6. By reducing the BEMF, a higher wind speed can be generated from a higher fan rotational speed. Table 6 shows that the HO dimension of 2.4 mm produces a smaller BEMF corresponding to the requirements, although the cogging torque is more significant, compared to the change in WO. In this Section, 2.4 mm is selected as a fixed factor.

Table 6 Cogging torque and BEMF data for different HO dimensions

HO (mm)	Cogging torque (N·m)	BEMF (V)	
1.8	0.0527	Phase1	5.241
		Phase2	5.326
		Phase3	5.317
		Average	5.295
2	0.0567	Phase1	5.197
		Phase2	5.281
		Phase3	5.272
		Average	5.250
2.4	0.0660	Phase1	5.098
		Phase2	5.183
		Phase3	5.175
		Average	5.152

2.2.3. Influence of different HS dimensions on torque and BEMF

This section primarily examines the effects of different HS sizes at 15.3, 15.0, and 14.7 mm on cogging torque and BEMF. The data for cogging torque and BEMF at panoply HS dimensions is presented in Table 7. Adjustments are performed to HS to reduce the cogging torque since, in the previous two Sections, the BEMF parameters were reduced to produce a higher cogging torque than the original value. The cogging torque seemed to decrease to 0.0449 N·m at an HS size of 14.7 mm, which is lower than the original value of 0.0505 N·m. Furthermore, Table 7 manifests that the BEMF decreases to 5.317V for the same HS size of 14.7 mm, which is also lower than the original value of 5.343V. Although the BEMF at 14.7 mm HS size is higher than that at 15.3 mm HS size (5.152V), a slight increase in BEMF is acceptable to reduce cogging torque.

Table 7 Cogging torque and BEMF data for different HS dimensions

HS (mm)	Cogging torque (N·m)	BEMF (V)	
15.3	0.0660	U1	5.098
		U2	5.183
		U3	5.175
		Average	5.152
15.0	0.0545	U1	5.185
		U2	5.269
		U3	5.260
		Average	5.238
14.7	0.0449	U1	5.264
		U2	5.348
		U3	5.339
		Average	5.317

2.3. Results and discussion of existing mechanism

Fig. 7 exhibits the comparison of the original and optimized cogging torque waveforms. The cogging torque has been found to be improved. The peaks and valleys of the waveforms have been reduced, and the waveforms are more harmonic than they were initially. The optimized cogging torque value is seemingly lower than the original value, where it was reduced from 0.0505 N·m to 0.0448 N·m. Reducing cogging torque has several positive effects on motor operation, including minimizing vibration, reducing bearing losses, and ultimately extending the overall lifespan of the motor. Therefore, reducing vibration will also help reduce noise. Fig. 8 shows that the improvement in BEMF is less significant than cogging torque. From the perspective of waveforms, a scarce difference between the original and optimized waveforms emerges. Apropos voltage value, the optimized BEMF is slightly lower than the original BEMF, decreasing from 5.316V to 5.261V.

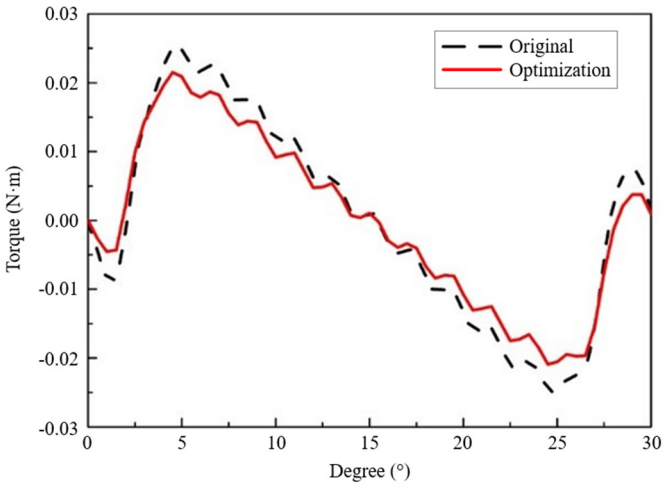

Fig. 7 Original and optimized cogging torque waveforms

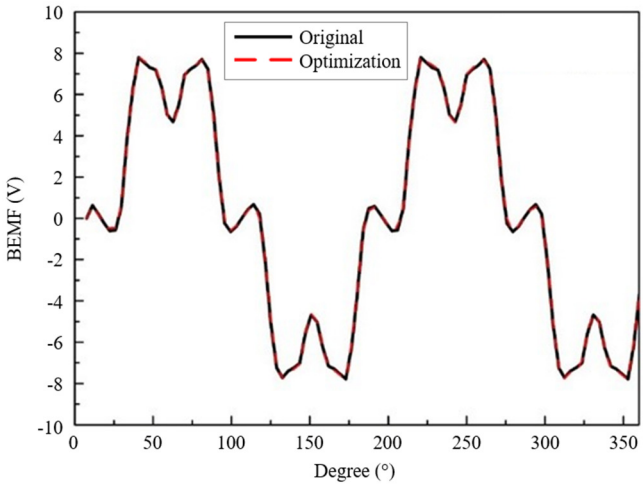

Fig. 8 Original and optimized BEMF waveforms

Theoretically, the reduction of BEMF can expedite the rotating speed. The overall effect is insignificant since the BEMF is barely reduced. According to the product specification, the maximum speed is estimated to be 8,600 rpm under the voltage value of 24 V DC. However, the improved BEMF only increases the speed by about 100 rpm and provides negligible assistance to increase performance. To ensure that the cogging torque adjustments will not cause the motor to fail to operate correctly, a torque analysis is required on the improved motor to determine if the torque is within a reasonable range. The calculated torque is 0.12 N·m, which is slightly lower than the original torque of 0.1216 N·m, whereas the optimized torque remains within the range required for regular operation. Fig. 9 compares the torque waveforms between the original and optimized motors, which evinces little difference and indicates limited operational influence.

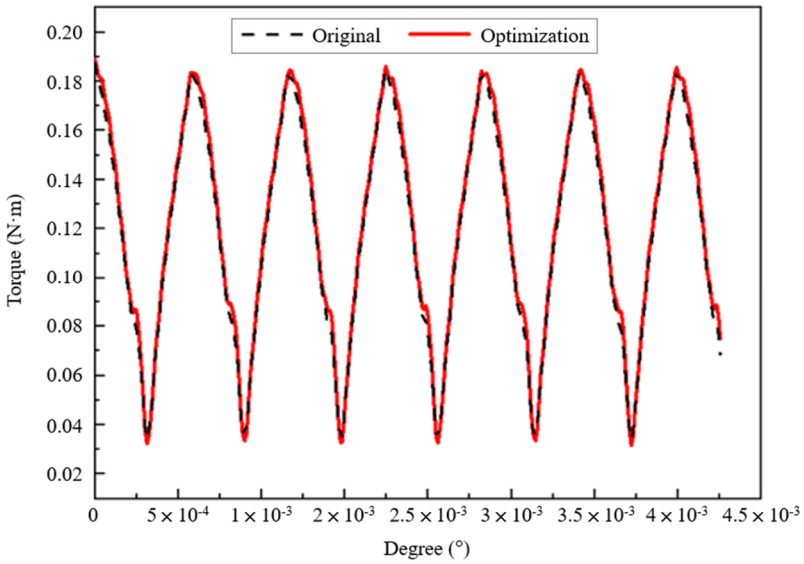

Fig. 9 Original and optimized Torque waveforms

In addition to the electromagnetic problem, a thermal problem emerges in the operation of the motor. Therefore, the presence of a problem in the magnetic field is examined when the motor is operating. Fig. 10 indicates the magnetic field distribution during motor operation. A denser distribution of the magnetic field is presented outside the rotor, which may signify the problem of magnetic saturation. Therefore, the magnetic flux density can be further examined during operation. Fig. 11 renders the magnetic flux density of the motor during operation. The places with higher magnetic flux density are accompanied by a denser distribution of magnetic lines. The flux density of the stator is within 2T, which is reasonable. The flux density in the teeth is high, and the highest flux density in the teeth is proximate to 2T. Since the maximum magnetic saturation of the 35CS550 material is 2T, the energy will be dissipated by heat if it exceeds 2T. Meanwhile, operation over a long time may generate excessive heat. As a fan motor with airflow directed to the stator, the effect of heat dissipation is expected to be minimal.

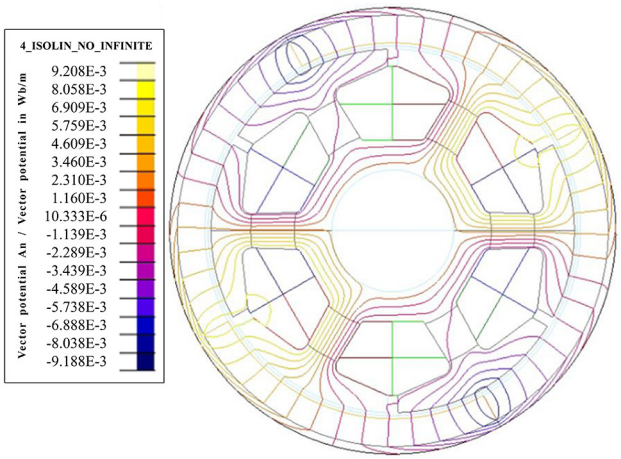

Fig. 10 Optimized motor magnetic field line distribution

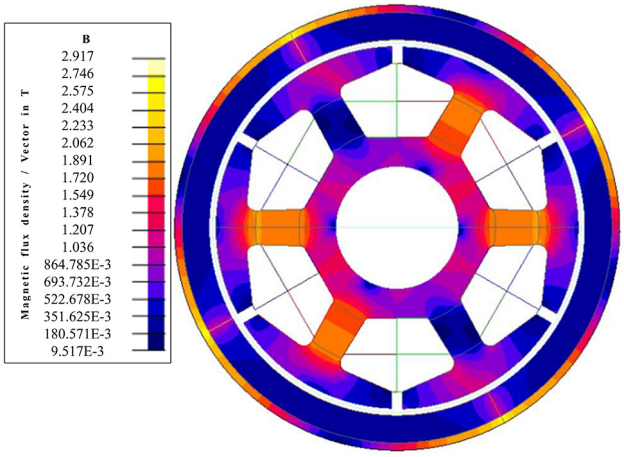

Fig. 11 Optimized motor flux density

3. Experimental Results and Discussion

In this paper, the geometry of the designed motor is modeled and manufactured using SolidWorks software. The silicon steel sheets are precisely cut to the required dimensions using wire-cutting techniques. These sheets are subsequently stacked to the designed thickness and integrated with the insulating frame. Copper wires are wrapped around this assembly accordingly. The resistance of the motor is measured to ensure accuracy after the completion of the winding process, and finally, warped wires are connected to the Δ configuration. Notably, the stator of the motor consists of 40 stacked silicon steel sheets with a thickness of 0.35 mm. After the insulating frame is glued on, the concentrated overlapping method is used to wrap 114 turns of copper wire with two 0.4 mm wires. The completed winding results in 12 outgoing wires; every two wires are considered one unit. Thus, six units are presented, three of which serve as input and output coils.

After completion of the winding process, the wire resistances of these three coils are measured to ensure uniformity and normality. The resistance and inductance of the three coils are confirmed by the Inductance, Capacitance, and Resistance (LCR) meter, and the results are presented in Table 8. According to measurements, no significant difference is observed in the resistance and inductance of each wire. The average wire resistance is 1.2598 Ω, while the average wire inductance is determined to be 2.6165 mH. By measuring line resistance and line inductance, the winding method is known to be correct. After the connection of Δ is completed, the measurement of three-phase resistance and inductance are carried out in Table 9. The analysis of these results reveals no significant difference in the resistance and inductance of each phase. The average phase resistance is calculated as 0.8195 Ω, while the average phase inductance is determined to be 2.4078 mH. Based on the above test results, it is confirmed that no significant error emerges in the production of the motor samples.

Table 8 Line resistance and inductance measurement results

	Resistance	Inductance
Coil windings A	1.2768 Ω	2.6225 mH
Coil windings B	1.2518 Ω	2.6097 mH
Coil windings C	1.2508 Ω	2.6173 mH
Average	1.2598 Ω	2.6165 mH

Table 9 Phase resistance and inductance measurement results

Phase	Resistance	Inductance
U	0.81656 Ω	2.4042 mH
V	0.82027 Ω	2.4097 mH
W	0.82168 Ω	2.4096 mH
Average	0.8195 Ω	2.4078 mH

Fig. 12 manifests the images of the fan assembly, which consists of two bearings, a spring, a C-ring, a washer, an external rotor fan, the motor stator, and a bracket. The fan generates a downward airflow and upward thrust during the operation. The function of the spring is to reduce upward thrust. The outer rotor and the fan are in one piece with a shaft between them and supported by bearings at the top and bottom ends. Thus, the torque vibration can potentially affect the bearings, resulting in a reduction in bearing life. Fig. 13 compares the BEMF between the original fan and the optimized fan. It signifies a slight decrease in the BEMF of the optimized fan, compared to the original fan. Since the analysis has known that the reduction in BEMF is insignificant, the experimental results confirm the feasibility of the simulation.

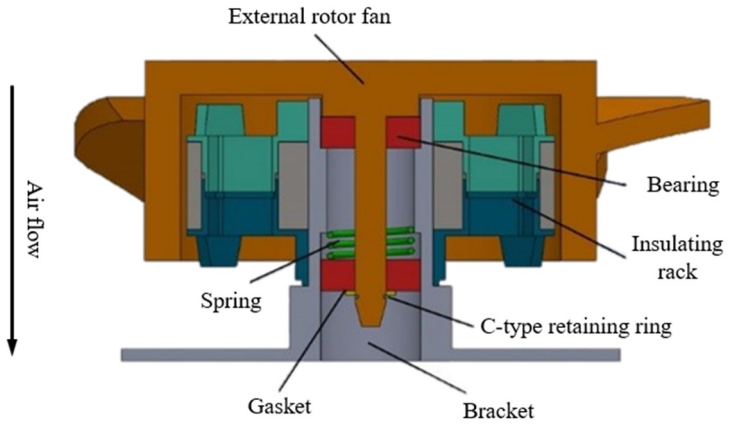

Fig. 12 Overall view of the fan

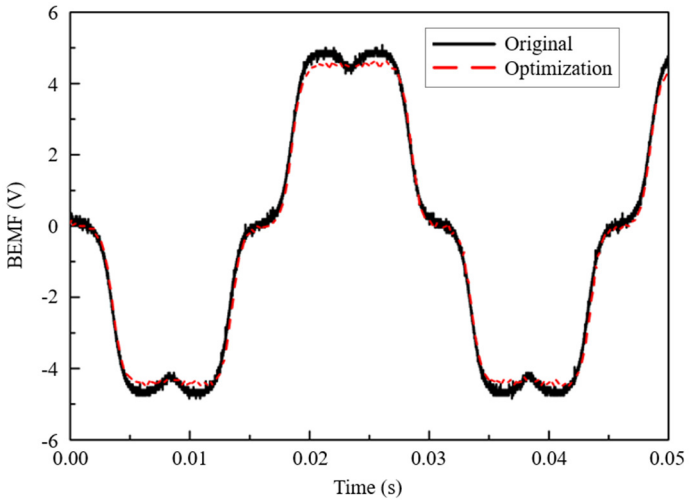

Fig. 13 Comparison of BEMF: original vs. optimized fan

Table 10 exhibits the comparative data of the speed measurement. Since the original fan and driver are one unit and can only be controlled by the pulse-width modulation (PWM) duty cycle, the minimum achievable speed is 2,000 rpm, and the maximum speed is 8,600 rpm. In this study, the DRV-8312 was used as the motor driver to provide speed control, and the results show that the optimized motor can operate stably below about 6,500 rpm. In addition, the optimized fan yields an increase in speed of about 8.8% compared to the original fan at 0.38A. Due to the tool conditions of the DRV-8312 driver, the controllability is hampered when the speed is above 6,500 rpm.

Table 10 The comparison of speed measurement results

Original fan			Optimized fan	
Current (A)	PWM duty cycle	Speed (rpm)	Current (A)	Speed (rpm)
0.38	0.2	3,300	0.16	1,800
0.69	0.4	4,600	0.38	3,592
1.6	0.69	6,570	0.71	4,800
2.06	0.8	7,320	1.57	6,489
2.98	0.98	8,500	1.58	6,521
-	-	-	1.59	6,593

However, Fig. 14 shows a comparative analysis of the speed measurements between the original and optimized fans. From the figure shown, the current required by the optimized fan is seemingly smaller than that of the original fan at low speed, which means that the optimized fan is more energy-saving at low speed. Furthermore, Fig. 14 demonstrates that the redesigned motor is controllable with a speed below 2,000 rpm. If the automatic winding machine makes the stator coil wiring, outperforming the original motor, as discussed in the simulation session, is predictably achievable.

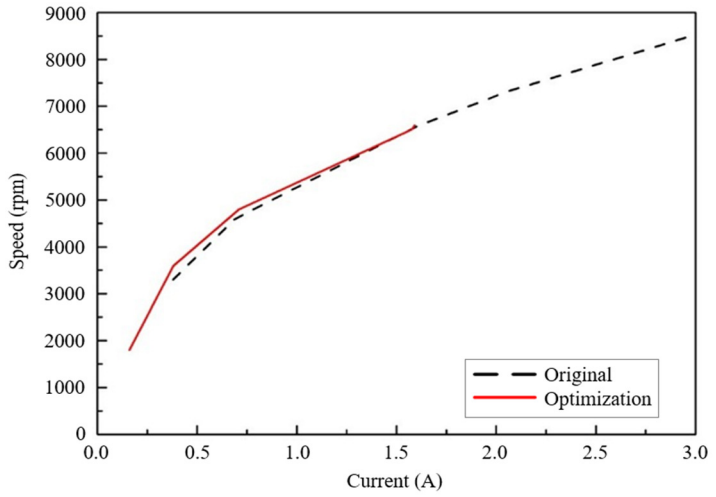

Fig. 14 The comparison chart of the original fan and optimized fan speed measurements

4. Conclusions

In this paper, the proposed method has been applied to obtain an enhanced stator design for the axial fan BLDC motor. It verifies the simulation results and feasibility of better design through motor manufacturing experiments. The Taguchi method was proposed to optimize the analysis of the influence of various motor components on cogging torque and BEMF. Furthermore, the most suitable combination of stator dimensions was determined by employing the one-factor-at-a-time, instrumentally reducing both cogging torque and BEMF while maintaining torque performance. Compared with the original fan motor, the proposed design can enhance the performance of the original motor by approximately 10% and improve the possibility of operation below 3,000 rpm. The simulation results render conclusive findings regarding three essential design parameters:

(1) The dimensions of the slot opening exhibit an inverse relationship with cogging torque and a direct relationship with BEMF.
(2) The toe dimensions showcase a direct relationship with cogging torque and an inverse relationship with BEMF.
(3) The dimensions of the slot depth demonstrate a direct relationship with cogging torque and an inverse relationship with BEMF.

The simulation and experiment results attested that changing the geometric dimension can only change the BEMF slightly. If a significant change in the BEMF is required, other design parameters require further consideration, such as the number of poles, the number of slots, the thickness of the magnet, the diameter of the winding wire, the turns of the wire, etc. In the future, the driver will be developed and combined with BLDC motors to effectuate fan products, which can be driven directly by PWM duty cycle signals. Subsequently, the proposed motor design can be compared concerning performance with the original motor in the high-speed operation range.

Acknowledgment

This research was supported by the National Science and Technology Council of the Republic of China under contracts NSTC 112-2221-E-230-002 and NSTC 112-2622-B-214-002.

Conflicts of Interest

The authors declare no conflict of interest.

References

[1] S. J. Chapman, Electric Machinery Fundamentals, 5th ed., New York: McGraw-Hill, 2012.
[2] C. L. Xia, Permanent Magnet Brushless DC Motor Drives and Controls, Hoboken, N.J.: Wiley-Science Press, 2012.
[3] Rupam, S. Marwaha, and A. Marwaha, "FEA Based Design of Outer Rotor BLDC Motor for Battery Electric Vehicle," International Journal of Electrical and Electronics Research, vol. 10, no. 4, pp. 1130-1134, 2022.
[4] A. Nandhakumar, K. V. Santhoshkumar, T. Alexstanley Raja, J. C. Rithiya Sonaa, S. Kavya, and S. Swetha, "Design and Analysis of Brushless DC Motor for Pure Electric Vehicle," International Journal of Electrical Engineering and Technology, vol. 13, no. 5, pp. 19-25, 2022.
[5] T. Vijay, B. R. Naveen Gowda, H. Farman, S. Praveen, and N. S. Sunitha, "Design of Brushless DC Motor for Electric Vehicle," Journal of Emerging Technologies and Innovative Research, vol. 7, no. 10, pp. 56-61, 2020.
[6] N. B. Hung and O. Lim, "A Review of History, Development, Design and Research of Electric Bicycles," Applied Energy, vol. 260, article no. 114323, 2020.
[7] Z. Arifin, I. W. Adiyasa, and M. A. Hizami Rasid, "Design Optimization Analysis on the Performance of BLDC Motors on Electric Bicycles," Journal of Physics: Conference Series, vol. 2406, article no. 012016, 2022.
[8] S. Magibalan, C. Ragu, D. Nithish, C. Raveeshankar, and V. Sabarish, "Design and Fabrication of Electric Three-Wheeled Scooter for Disabled Persons," Materials Today: Proceedings, vol. 74, part. 4, pp. 820-823, 2023.

[9] S. R. Salehinai, E. Afjei, A. Hekmati, and H. Aghazadeh, "Design Procedure of an Outer Rotor Synchronous Reluctance Machine for Scooter Application," International Journal of Engineering, vol. 34, no. 3, pp. 656-666, 2021.
[10] M. Aishwarya and R. M. Brisilla, "Design of Energy-Efficient Induction Motor Using ANSYS Software," Results in Engineering, vol. 16, article no. 100616, 2022.
[11] M. Appadurai, E. Fantin Irudaya Raj, and K. Venkadeshwaran, "Finite Element Design and Thermal Analysis of an Induction Motor Used for a Hydraulic Pumping System," Materials Today: Proceedings, vol. 45, part 7, pp. 7100-7106, 2021.
[12] S. Brisset and P. Brochet, "Analytical Model for the Optimal Design of a Brushless DC Wheel Motor," The International Journal for Computation and Mathematics in Electrical and Electronic Engineering, vol. 24, no. 3, pp. 829-848, 2005.
[13] C. Das, M. B. Ullah, M. Asaduzzaman, S. Ashraf, H. Kabir, and M. A. M. Chwdhury, "Design and Development of a Brushless Direct Current Motor," International Journal of Scientific Research and Engineering Development, vol. 2, no. 4, pp. 722-727, 2019.
[14] A. K. Singh, "Design and Performance Analysis of an Interior Permanent Magnet Brushless DC Motor Using ANSYS Electronics," International Journal of Advance Research, Ideas and Innovations in Technology, vol. 6, no. 1, pp. 255-260, 2020.
[15] K. Ren, H. Chen, H. Sun, Q. Wang, Q. Sun, and B. Jin, "Design and Analysis of a Permanent Magnet Brushless DC Motor in an Automotive Cooling System," World Electric Vehicle Journal, vol. 14, no. 8, article no. 228, 2023.
[16] M. Niaz Azari, M. Samami, and S. M. Abedi Pahnekollaei, "Optimal Design of a Brushless DC Motor, by Cuckoo Optimization Algorithm (Research Note)," International Journal of Engineering, vol. 30, no. 5, pp. 668-677, 2017.
[17] O. Tosun and N. F. O. Serteller, "The Design of the Outer-Rotor Brushless DC Motor and an Investigation of Motor Axial-Length-to-Pole-Pitch Ratio," Sustainability, vol. 14, no. 19, article no. 12743, 2022.
[18] S. A. Sadrossadat and O. Rahmani, "A Framework for Statistical Design of a Brushless DC Motor Considering Efficiency Maximisation," IET Electric Power Applications, vol. 16, no. 3, pp. 407-420, 2022.
[19] S. Bhuvaneswari, P. Sivaraman, N. Anitha, and A. Matheswaran, "Optimized Design of Permanent Magnet Brushless DC Motor for Ceiling Fan Applications," Materials Today: Proceedings, vol. 45, part 2, pp. 1081-1086, 2021.
[20] K. S. Thakur, P. S. Zamre, A. A. Vasaikar, S. R. Sakharkar, and M. Dutta, "Design, Manufacturing and Analysis of Integrated Motor and Fan Assembly," International Journal of Engineering Research & Technology, vol. 9, no. 3, 2021.
[21] U. Sharma and B. Singh, "Design and Development of Energy Efficient Single Phase Induction Motor for Ceiling Fan Using Taguchi's Orthogonal Arrays," IEEE Transactions on Industry Applications, vol. 57, no. 4, pp. 3562-3572, 2021.
[22] "Sanyo Denki 9SG5748P5G01 Datasheet," https://www.mouser.tw/datasheet/2/471/San_Ace_172SG51S_E-1287968.pdf, 2024.
[23] K. Kanagarathinam, R. Manikandan, and S. Ravivarman, "Impact of Stator Slot Shape on Cogging Torque of BLDC Motor," International Journal of Electrical and Electronics Research, vol. 11, no. 1, pp. 54-60, 2023.
[24] A. N. Patel, "Slot Opening Displacement Technique for Cogging Torque Reduction of Axial Flux Brushless DC Motor for Electric Two-Wheeler Application," Electrical Engineering & Electromechanics, no. 2, pp. 7-13, 2023.
[25] H. Prajapati and G. Tapiawala, "Performance Analysis of Brushless DC Motor," IEEE 3rd Global Conference for Advancement in Technology, pp. 1-8, 2022.
[26] D. C. Hanselman, Brushless Permanent Magnet Motor Design, 2nd ed., Lebanon, Ohio: Magna Physics Publishing, 2006.